Electrical steel dynamic behavior quantitated by inductance spectroscopy: toward prediction of magnetic losses

Benjamin Ducharne, S. Zhang, Gaël Sebald, S. Takeda, T. Uchimoto

Electrical steel dynamic behavior quantitated by inductance spectroscopy: toward prediction of magnetic losses

B. Ducharne[1, 2, ✉], S. Zhang[2, 3], G. Sebald[1], S. Takeda[3], T. Uchimoto[1, 3]

1. ELyTMaX UMI 3757, CNRS – Université de Lyon – Tohoku University, International Joint Unit, Tohoku University, Sendai 980-8577, Japan
2. LGEF, INSA Lyon, 69621 Villeurbanne, France
3. Tohoku University, Institute of Fluid Science IFS, Sendai 980-8577, Japan

✉ corresponding author: benjamin.ducharne@insa-lyon.fr

Abstract

Energy conversion is essential to meeting sustainable energy needs. Higher frequencies impart enhanced efficiency. Standard magnetic characterization methods have not been designed for these working conditions, and manufacturers seek alternative solutions.

Inductance spectroscopy (IS), which is easy to implement in a production line, relies on impedance measurements during frequency sweeps. IS gives access to dynamic behaviors. Combined with dedicated simulation methods, IS enables parameters that are useful for predicting the hysteresis cycle frequency dependence and the related magnetic losses to be set.

We applied IS to oriented grains of electrical steels. We established a correspondence between a lumped model developed to simulate hysteresis cycles and the magnetic version of the Cole–Cole ferroelectric method for IS.

We obtained good comparisons with experimental results on large frequency bandwidths for both models and with the same combination of dynamic parameters. We established the uniformity of the dynamic behavior, such as the possibility to characterize this behavior by IS.[1]

Keywords: Dynamic hysteresis, Cole–Cole model, fractional derivative, impedance analysis

[1]GO: oriented grains; ImS: impedance spectroscopy; IS: inductance spectroscopy; RD: rolling direction; STL: statistical theory of losses; TD: transverse direction.

1 – Introduction

Energy efficiency is essential to meeting clean energy needs. Although solar and other renewable energy technologies usually take precedence, energy efficiency also lowers emissions [1], and researchers predict substantial progress [2]. There are multiple possibilities for this progress, including new geometrical designs, materials, and technologies.

We focus explicitly on magnetic conversion, magnetic loss evaluation, and characterization. Magnetic loss prediction in electromagnetic devices is a longstanding problem [3][4]. Nevertheless, the large number of recent papers is noteworthy, confirming a resurgence of interest that is motivated by sustainability and electrification in the transportation domain [5]-[10].

Progression in industrial development proceeds through technological breakthroughs, which can be listed as follows (in the context of magnetic laminated cores).

- Silicon adjunction
- Goss texture [11]
- Stacking [12]
- Coating [13]

These advances have substantially improved energy efficiency. Nevertheless, research is still ongoing. In 2014, the World Bank database estimated that 8% of the world's electrical energy production was lost between generation and consumption [14]. Of that 8%, one can attribute a considerable fraction to magnetic conversion, hysteresis, and eddy current loss.

If nothing is done to reduce this waste, the fraction of energy lost will increase with the spread of high-frequency-power electronics, which will require an alternative means of power distribution [15][16].

High-frequency characterization is necessary for the development of high-frequency magnetic cores. Magnetic characterization standards describe the necessary experimental conditions for measuring the magnetic hysteresis cycles: evolution of the cross-section averaged induction $\mathbf{B}_a$ as a function of the tangent surface magnetic excitation field $\mathbf{H}_{surf}$. For electrical steels, these standards include:

- Epstein frame (IEC 60404 – 2 [17]);
- Single-sheet tester (IEC 60404 – 3 [18]); and
- Toroidal magnetic core (IEC 60404 – 6 [19]).

Among these methods, IEC 60404-6 is the only one that mentions the high-frequency range (higher than a few hundred hertz). Nevertheless, this technique imposes toroidal-shaped specimens, which is never the case on a production line.

Further advances in magnetic characterization are needed. Inductance spectroscopy (IS) is pertinent in this context. IS has rarely been used in industry and, to our knowledge, never for electrical steel. However, IS has been demonstrated on amorphous materials [20] to be an accurate means of characterizing the behavior of soft ferromagnetic materials in the high-frequency range. IS can easily be implemented for fast, nondestructive controls because it only requires an impedance analyzer and good electrical contacts.

In this study, we used IS to observe the dynamical behavior of grain-oriented (GO) electrical steel (FeSi) laminated strips. We also developed an IS simulation method based on the

ferromagnetic version of the classical ferroelectric Cole–Cole model. We established a relationship between this simulation method and a lumped model based on a fractional differential equation that was previously revealed to be efficient for simulating the hysteresis losses (high-amplitude, frequency-dependent hysteresis cycles as observed with standard characterization techniques).

From this relationship we developed conclusions, including the consistency of the dynamic behavior observed from IS and the possibility of assessment by this characterization method.

This manuscript is organized as follows. The second section presents IS. Subsections are dedicated to the experimental setup and the tested specimens. The third section presents the experimental results. The fourth section presents the simulation method (Cole–Cole model), such as its relation with the lumped model based on a fractional differential equation. The fifth section presents the discussions and conclusions.

2 – Inductance spectroscopy, description, and implementation

Researchers have implemented impedance spectroscopy (ImS) to investigate the ferroelectric properties of many materials (e.g., metallic [21], ceramic [22], and polymeric [23]). ImS is rapid, nondestructive, and can be easily automated. ImS applies frequency sweeps of an imposed sinusoidal voltage/current and monitors the current/voltage responses. The resulting impedance $\mathbb{Z}$ is a powerful indicator of the material properties [24]. IS, described next, is the magnetic complement of ImS. It is based on the same ideas but focuses on magnetic properties.

2.1 - Inductance spectroscopy: description

IS outputs the evolution of the inductance L as a function of frequency. Initial research on this topic was carried out in the middle of the twentieth century [25]. IS is a versatile means of characterizing the magnetization dynamics of soft ferromagnetic materials (e.g., amorphous ribbons and wires [26][27], ferrites [25], and glass-coated ferromagnetic microwires [28]).

Similarly to ImS, IS relies on impedance analyzer equipment. IS monitors the impedance of sensor coils, which can have various geometries.

- Flat pancake coil (Fig. 1) positioned parallel and close to the surface of a ferromagnetic specimen.

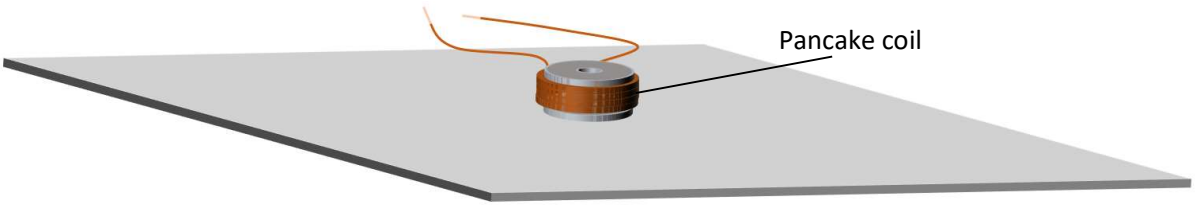

Fig. 1 – Pancake coil sensor.

- Ferromagnetic sample, subjected to an alternating current (AC) (Fig. 2). In this configuration, the magnetic excitation comes from the alternating electrical current flowing in the tested specimen.

One exciting property of IS (in the context of ferromagnetic thin films) is its ability to distinguish the magnetization mechanisms [20]. These mechanisms can be regrouped into five families:

- Domain wall bulging (low $\mathbf{H}_{surf}$ amplitude range)[29];
- Domain wall irreversible motions (middle $\mathbf{H}_{surf}$ amplitude range)[30];
- Magnetization rotation (high $\mathbf{H}_{surf}$ amplitude range)[31];

- Domain wall frequency dependence, ripples, and avalanches phenomena (AC $\mathbf{H}_{surf}$)[32]-[34]; and
- Macroscopic eddy currents (AC $\mathbf{H}_{surf}$)[35].

Each of these mechanisms is characterized by its own time constant. All the magnetization mechanisms contribute in the low-frequency range, and the inductance value is maximal. The mechanisms associated with the domain wall motions (bulging, irreversible motions, etc.) are characterized by a high-time-constant. High-time-constant (slow dynamic) mechanisms cannot respond to the magnetic excitation when the frequency increases, leading to an incremental decrease in inductance. Each decrement and corresponding frequency is attributable to a given magnetization mechanism. Beyond a threshold frequency (relaxation frequency), the permeability becomes very small, reflecting the contribution of the magnetization rotation (characterized by a low-time-constant) as the only active magnetization mechanism. The time constant of the macroscopic eddy current is easier to assess as the equations associated with this mechanism are well known. Finally, a careful study of the inductance variations yields essential information about the magnetization processes.

2.2 - Inductance spectroscopy: experimental setup description

Fig. 2 shows a photograph and a schematic three-dimensional view of the experimental setup that we designed to characterize electrical steel strips by IS.

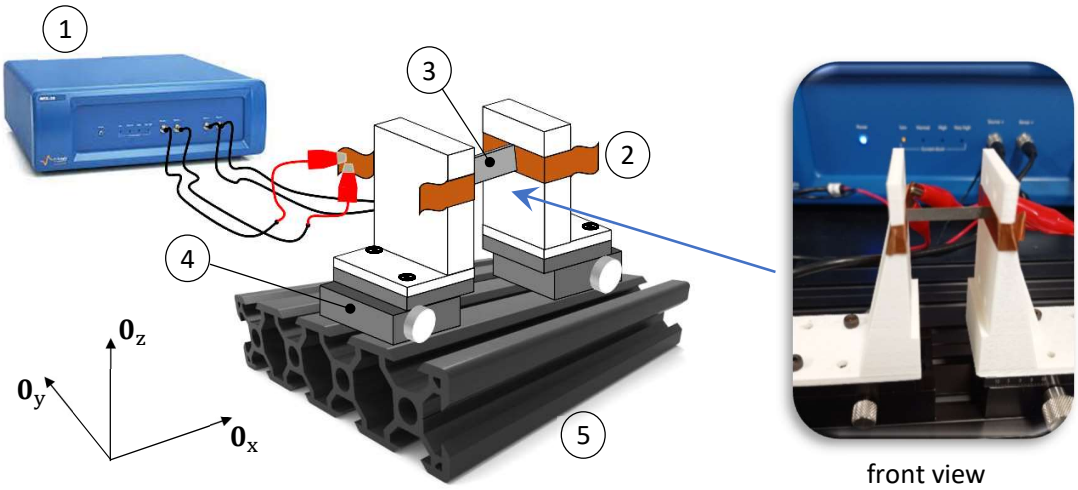

1 Impedance analyzer
2 Copper tape
3 GO FeSi specimen
4 Linear actuator
5 Aluminum rail

Fig. 2 – Photograph and overall three-dimensional view of the experimental setup.

The tested specimen was placed between two electrodes (copper tape, n°2 in Fig. 2). The contact resistances associated with the copper tape electrodes were compensated through a pre-calibration step. Two linear actuators translating in the $\mathbf{O}_x$ direction were used to ensure excellent electrical contacts. Four-point impedance measurements (where current-carrying and voltage-sensing electrodes are separated) were achieved with the impedance analyzer. BioLogic MTZ35 (Grenoble, France) and NF Corporation ZM2375 (Yokohama, Japan) analyzers were tested to check the results' reproducibility. The voltage- and current-imposed experiments were tested; Since the analyzer output impedance is much larger than the specimen one, working under the voltage-imposed is equivalent to working under the current-imposed, and similar plots were obtained. The complex inductance was calculated in post-processing using Eq. (1) and Eq. (2) [36].

$$\mathbf{L} = -\mathrm{j}\frac{\mathbf{Z}}{\omega} \tag{1}$$

$$\mathbf{L} = \mathrm{L}' + \mathrm{jL}'', \tag{2}$$

where $j = \sqrt{-1}$, ω is the angular frequency, L' and L'' the real and the imaginary part of the inductance $\mathbf{L}$.

2.3 - Tested specimens

All of the tested specimens were from the same batch and were all GO FeSi laminated strips with 3 wt % silicon content. Table 1 shows the physical properties measured at room temperature for GO FeSi as gathered from the manufacturer's website.

Table 1 – Typical values of FeSi GO magnetic parameters at room temperature.

	Composition	Max. relative permeability (μ_{max})	Coercive field Hc ($A \cdot m^{-1}$)	Saturation polarization Js(T)	Curie Temperature Tc (°C)	Saturation magnetostriction $\lambda_s=(\Delta l/l)_{Js}$
GO FeSi	Fe_{97}–Si_3	(15–80) × 10^3	4–15	2.02	750	(1–3) × 10^{-6}

	Core loss ($W \cdot kg^{-1}$)					
	W10/50	**W10/400**	**W10/1k**	**W5/2k**	**W1/10k**	**W0.5/20k**
GO FeSi	0.7	14.4	62.0	50.2	38.0	33.0

W10/50 is the core loss at 50 Hz, 1 T (10 kGauss)

GO FeSi specimens have strong magnetic anisotropy because of their Goss texture [11]. Fig. 3, right-hand side, shows this anisotropy; where simulations of the anhysteretic behavior [37] show $\|\mathbf{B}_{\text{a-anh}}\|$ for various angles and amplitudes of $\mathbf{H}_{\text{surf}}$. The left-hand side of Fig. 3 shows the tested specimens' geometrical characteristics.

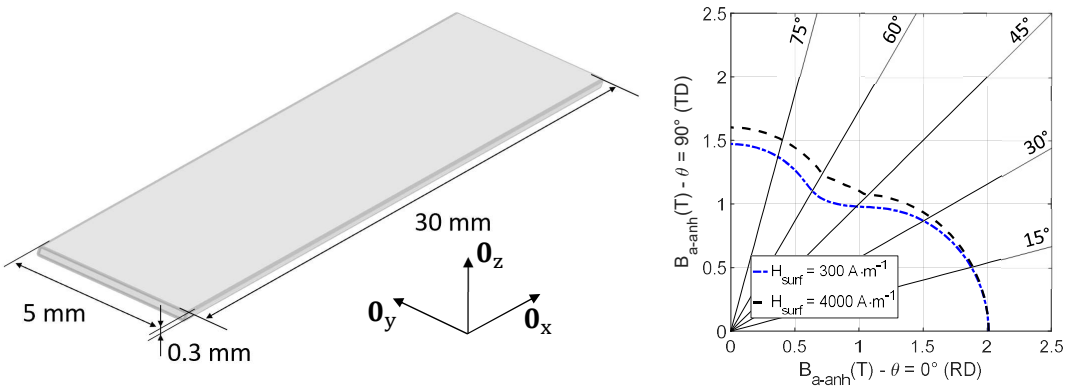

Fig. 3 – Specimen dimensions and illustration of the magnetic anisotropy in GO FeSi.

3 – Electrical steel: inductance spectroscopy and experimental results

Fig. 4 shows the experimental results obtained in current-imposed conditions and a maximum amplitude varying from 2 to 100 mA. The electrical current flowed in the transverse direction (TD).

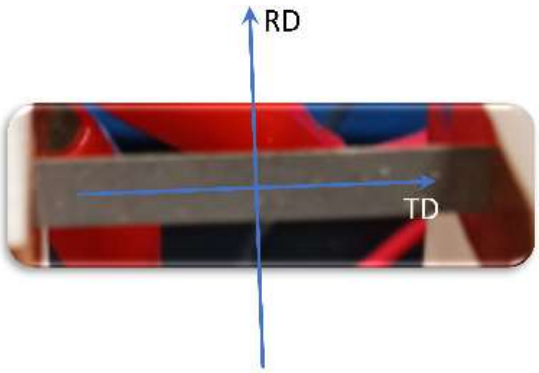

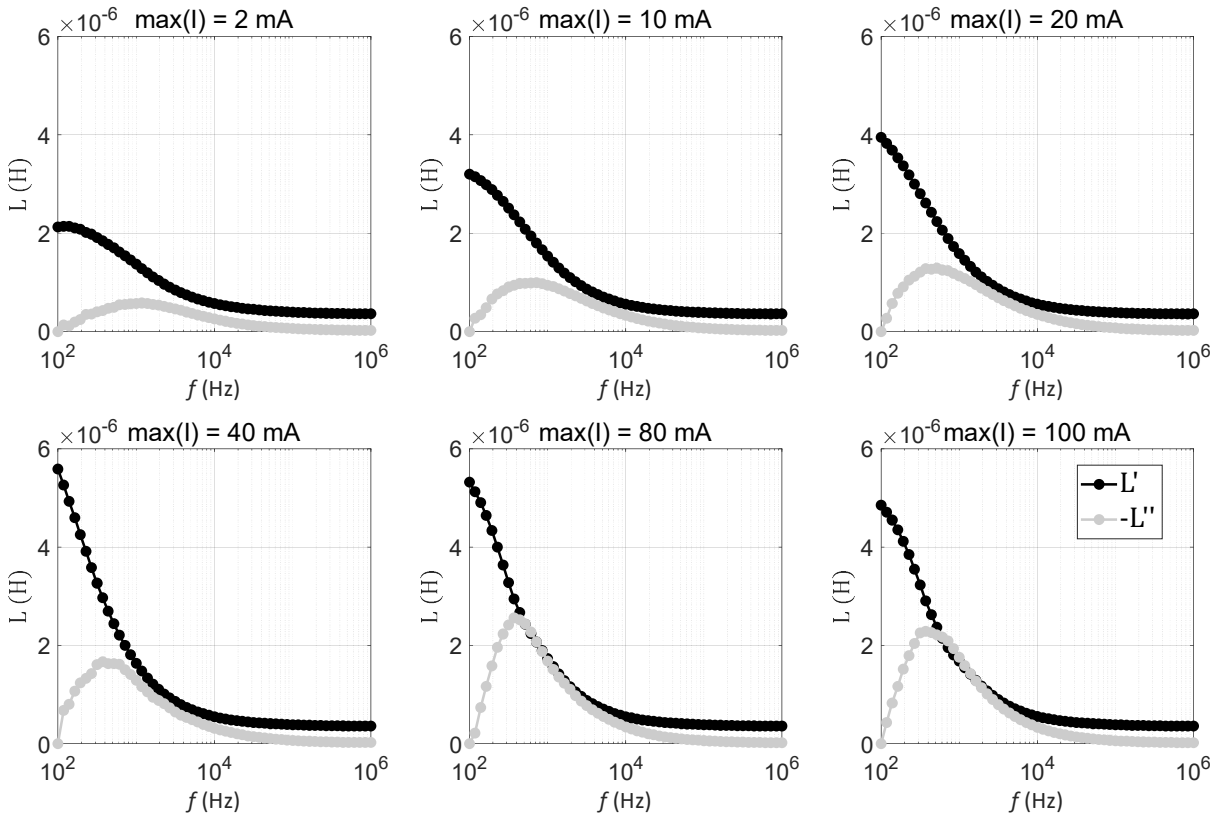

Fig. 4 – Real and imaginary parts of the relative effective permeability as a function of the excitation frequency; the electrical current flowed in the transverse direction.

Fig. 5 shows the results obtained in the same conditions, but in which the electrical current flowed in the rolling direction (RD).

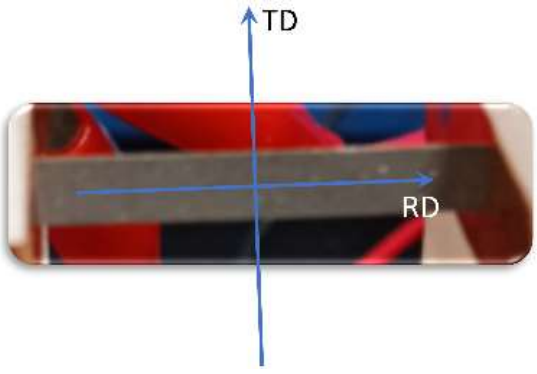

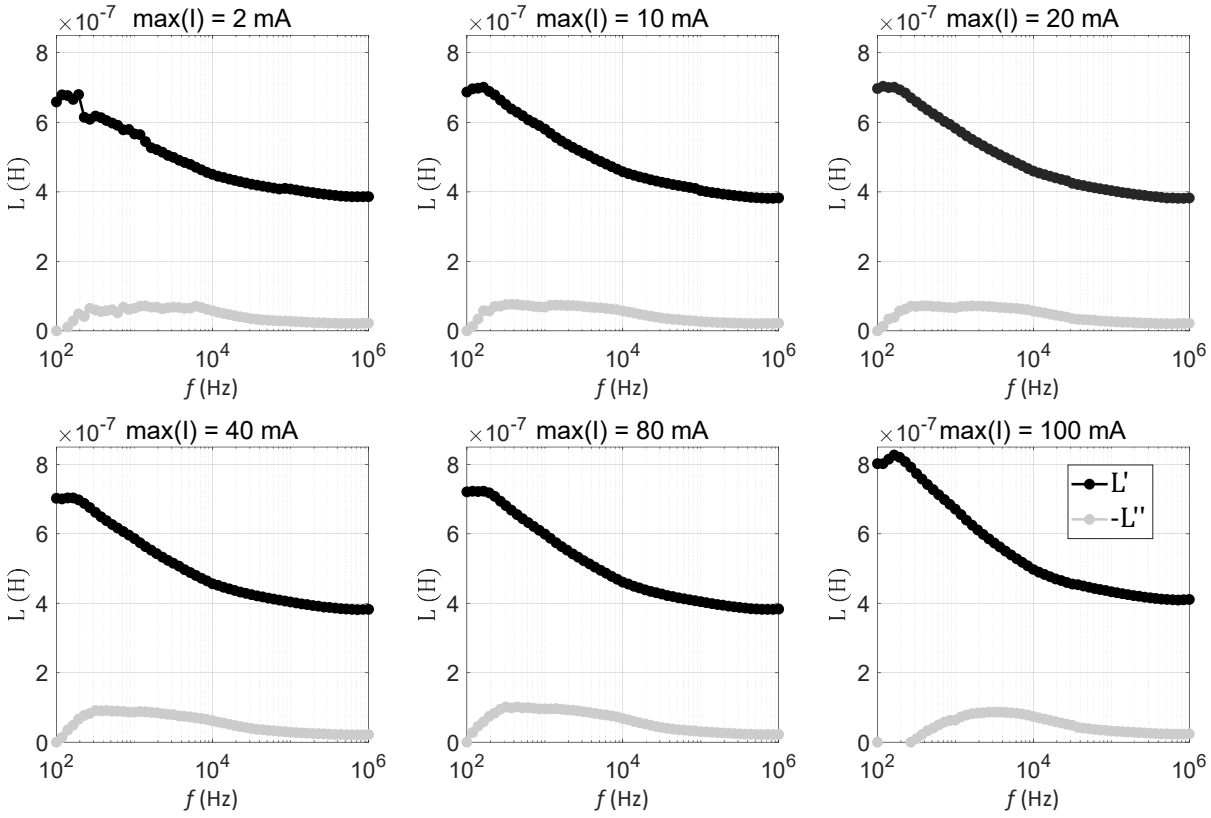

Fig. 5 – Real and imaginary parts of the relative effective permeability as a function of the excitation frequency; the electrical current flowed in the rolling direction.

Figs. 4 and 5 confirm a strong anisotropy in the magnetic response of the GO FeSi. When the electrical current flowed in the TD (Fig. 4), a resulting magnetic field was generated in the RD (easy magnetization axis), leading to high inductance values. This observation was especially true in the low-frequency range when the frequency is low enough to drive every magnetization mechanism. When the excitation amplitude is large, the resulting inductance is high, reflecting the superposition of all these mechanisms. Refs. [38] and [39] reveal that a magnetic field that is greater than at least half of the coercivity Hc ($\approx \in$ [5–20] $A \cdot m^{-1}$ in RD) is required to generate irreversible domain wall motions.

It is complex to estimate precisely the amplitude of the magnetic excitation field during the testing process. FeSi GO laminated sheets are characterized by stiff hysteresis cycles (Fig. 6);

saturation comes soon after coercivity under the influence of an increasing magnetic excitation field. The substantial difference between behaviors observed at 10 and 40 mA combined with the relative invariance for ≥40 mA indicates that a steady-state has been reached. An increase in the flowing current induces a rise in magnetic excitation, and the steady-state can be assimilated into a saturated state. This observation concludes that coercivity was reached in the 10- to 40-mA range. Fig. 6 shows a FeSi GO low-frequency range $\mathrm{B_a}(\mathrm{H_{surf}})$ hysteresis cycle. Nonlinear behaviors started at $\mathrm{H_{surf}}$ = 2·Hc, and saturation was reached at 3·Hc, which is in these conditions slightly greater than 50 A·m^{-1}. Fig. 6 shows a FeSi GO low-frequency range $\mathrm{B_a}(\mathrm{H_{surf}})$ hysteresis cycle. Nonlinear behaviors started at $\mathbf{H}_{\mathrm{surf}}$ = 2·Hc, and saturation was reached at 3·Hc, which is in these conditions slightly greater than 50 A·m^{-1}.

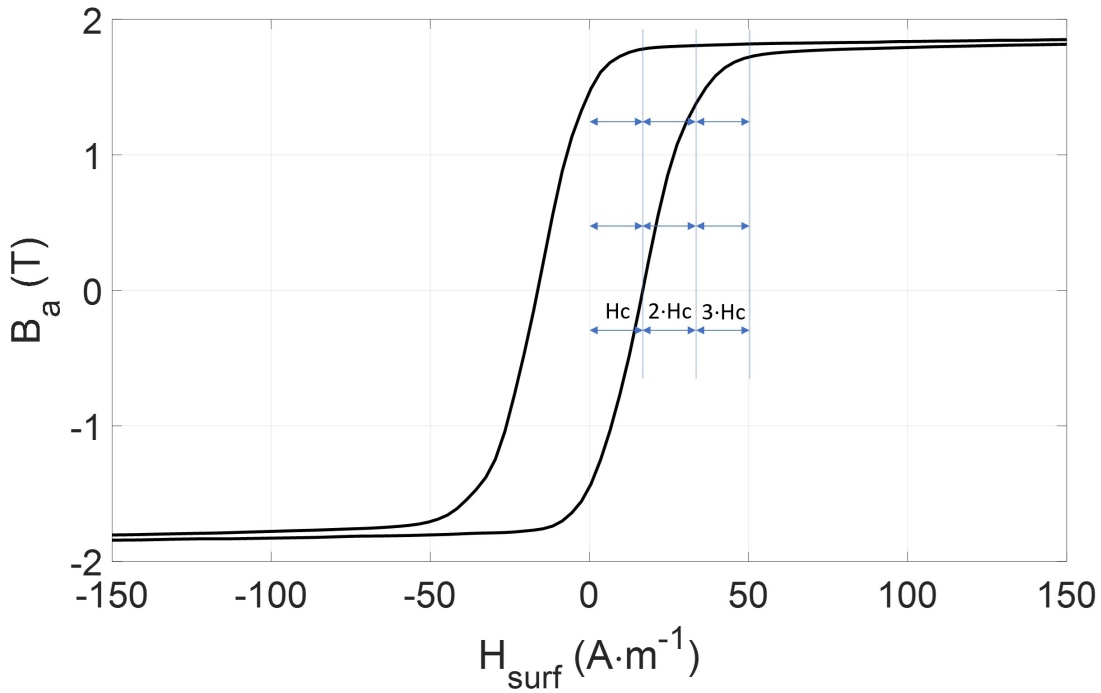

Fig. 6 – Quasi-static $\mathbf{B}_{\mathrm{a}}(\mathbf{H}_{\mathrm{surf}})$ hysteresis cycle for GO FeSi.

Coercivity increases with the frequency [40]. To reach coercivity and saturation in the 10^2–10^6 Hz range means larger $\mathbf{H}_{\mathrm{surf}}$ levels than those depicted in Fig. 6. Based on this observation, we

assumed that a maximum magnetic field of 100 A·m^{-1} when max(I) = 100 mA is probably close to the real practical condition.

It is interesting to observe the plateau-like behavior of L' in the low-frequency range of Fig. 5 and its quasi-absence when the excitation current was high in Fig. 4.

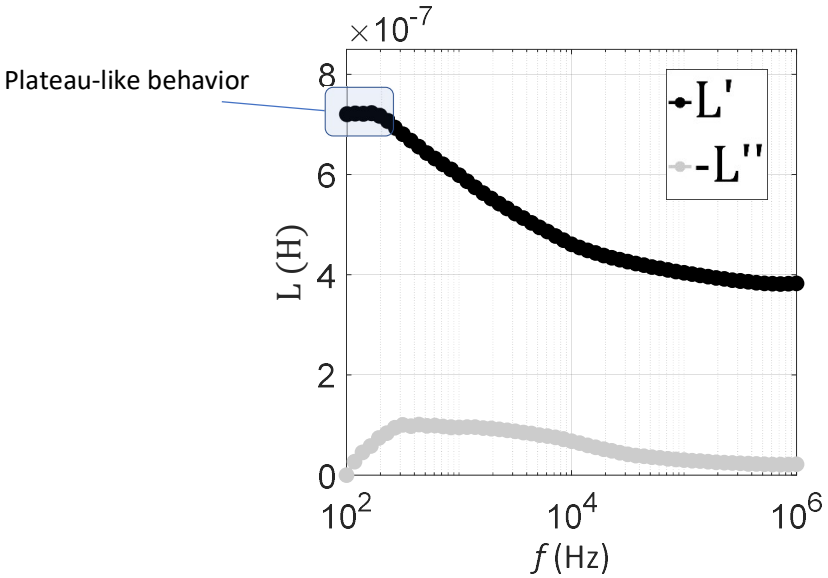

Fig. 7 – Illustration of plateau-like behavior.

This behavior is related to the domain wall bulging mechanism, characterized by a time constant that is lower than the other magnetization mechanisms. The contribution of domain wall bulging in terms of inductance was minimal, justifying its omission in most of the Fig. 4 curves where the macroscopic eddy currents' and the domain wall motions' contributions were dominant. Another plateau-like is observable for L' in the high-frequency range of all Fig. 4 and 5 charts. This plateau-like is associated with the magnetization rotation as it is the only mechanism of time constant low enough to be activated by the high frequencies tested. Researchers have reported such observations on ferromagnetic amorphous ribbons [20].

4 – Simulation tool: frequency dependence of the magnetic hysteresis cycles and inductance spectroscopy

This section reports our work with simulation tools on demonstrating the potential of IS as an experimental method for evaluating the magnetic losses and dynamic behavior of electrical steel. We focused on the high-frequency range where standard characterization methods indicate limitations.

We established a correspondence between simulation methods developed for the frequency dependence of the hysteresis cycles and those designed for the inductance.

4.1 - Fractional differential model for the frequency dependence of ferromagnetic hysteresis

In the 1980s, Bertotti described electrical steel magnetic loss in the Statistical Theory of Losses (STL) [4][41]. In accordance with the STL, one can delineate the magnetic loss into three contributions:

$$W = W_{hy} + W_{cl} + W_{ex}, \tag{3}$$

where:

- The quasi-static loss W_{hy} is frequency-independent and characteristic of the low-frequency range.
- The classic loss W_{cl} is linked to the macroscopic eddy currents. W_{cl} is derived from the Maxwell equations and is based on the assumption that skin effect is negligible:

$$W_{cl} = \frac{\sigma d^2}{12} \int_0^{1/f} \left(\frac{d\mathbf{B}_a}{dt}\right)^2 dt, \tag{4}$$

where σ is the electrical conductivity and d is the laminated sheet thickness.

- The excess loss W_{ex} is related to the magnetic domains kinetics:

$$W_{ex} = \sqrt{\sigma S g V_0} \int_0^{1/f} \left|\frac{d\mathbf{B}_a}{dt}\right|^{1.5} dt, \quad (5)$$

where g = 0.1356 is a dimensionless coefficient, S the cross-sectional area, and V_0 is a max($\mathbf{B}_a$)-dependent statistical parameter linked to the microstructure. The STL is a powerful means of estimating the ferromagnetic losses, but it assumes a full flux penetration, which restrains its domain of validity to a few hundred hertz. The STL is not applicable in this study, in which we targeted high-frequency behavior.

Space-discretized methods are good alternatives [32]-[34][42]. A one-dimensional resolution of a combination between the magnetic field diffusion equation (Eq. (6)) for the classic loss contribution and a viscosity-based magneto-dynamic model for both the hysteresis and excess loss contribution W_{ex} (Eq. (5)) gives excellent results. For this material law, a basic expression (Eq. (7)) can lead to a unique formulation (Eq. (8)) that is readily solvable by matrix inversion [33]:

$$\frac{\partial^2 H}{\partial^2 z} = \sigma \frac{dB}{dt} \quad (6)$$

$$\rho \frac{dB}{dt} = H(t) - H_{stat}(B) \quad (7)$$

$$\frac{\partial^2 H}{\partial^2 z} = \sigma \frac{H(t) - H_{stat}(B)}{\rho}, \quad (8)$$

where B and H are the projections on the magnetization axis of the magnetic induction and excitation fields, ρ is a constant, and z is in the thickness direction (Fig. 3). H_{stat} cannot be measured but can be calculated from a static model of material law [33]. More accurate results can be obtained with an improved formulation (Eq. (9)) [42]:

$$\frac{dB}{dt} = \frac{\delta}{g(B)} |H(t) - H_{stat}(B)|^{\alpha(B)}, \quad (9)$$

where δ is a directional parameter (= +/- 1), and we set the B-dependent functions $\alpha(B)$ and $g(B)$ by comparisons with experimental results. With such a high number of parameters, we obtained

excellent simulation results. However, this method resembles a fitting process; and thus requires a large quantity of experimental data and is complex to implement in industrial applications.

In this context of frequency limitations or excessively sophisticated techniques, alternative methods are needed. Consequently, some simulation techniques are based on mathematical operators in the framework of fractional derivatives. Researchers have tested various approaches, including the lump fractional differential equation (Eq. (10)) [43][44]; such as in extending both the Preisach and Jiles–Atherton quasi-static hysteresis models $\mathrm{H}_{\mathrm{stat}}(\mathbf{B}_{\mathrm{a}})$ to the frequency dependence through the adjunction of a fractional viscoelastic-type dynamic term:

$$\rho \frac{\mathrm{d}^{\mathrm{n}}\mathbf{B}_{\mathrm{a}}}{\mathrm{dt}^{\mathrm{n}}} = \mathbf{H}_{\mathrm{surf}}(\mathrm{t}) - \mathrm{H}_{\mathrm{stat}}(\mathbf{B}_{\mathrm{a}}), \tag{10}$$

where n is the fractional order.

Fig. 8 shows the hysteresis loss for various maximum sinusoidal magnetic induction levels and comparisons with simulation results (Eq. (10)). We obtained the experimental results from the literature [45]. After running the optimization process [46], we obtained good simulation results; ρ = 0.05 $\mathrm{A{\cdot}s^{n}{\cdot}T^{-n}{\cdot}m^{-1}}$ and n = 0.83.

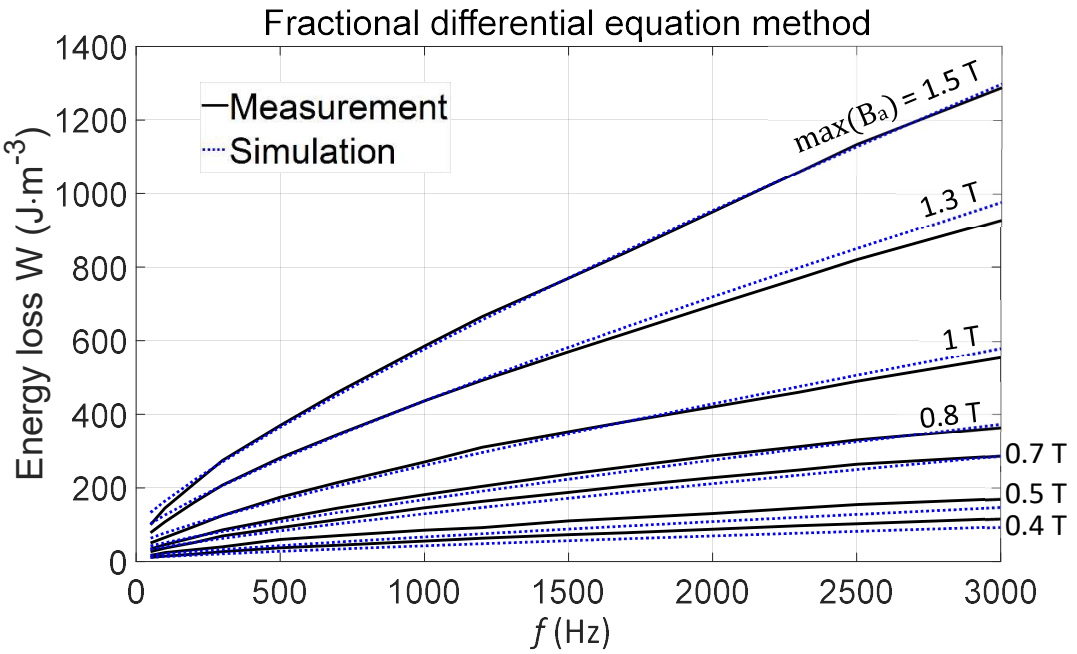

Fig. 8 – Comparison of simulations (fractional differential equation)/experimental results for the magnetic energy loss in a GO FeSi specimen.

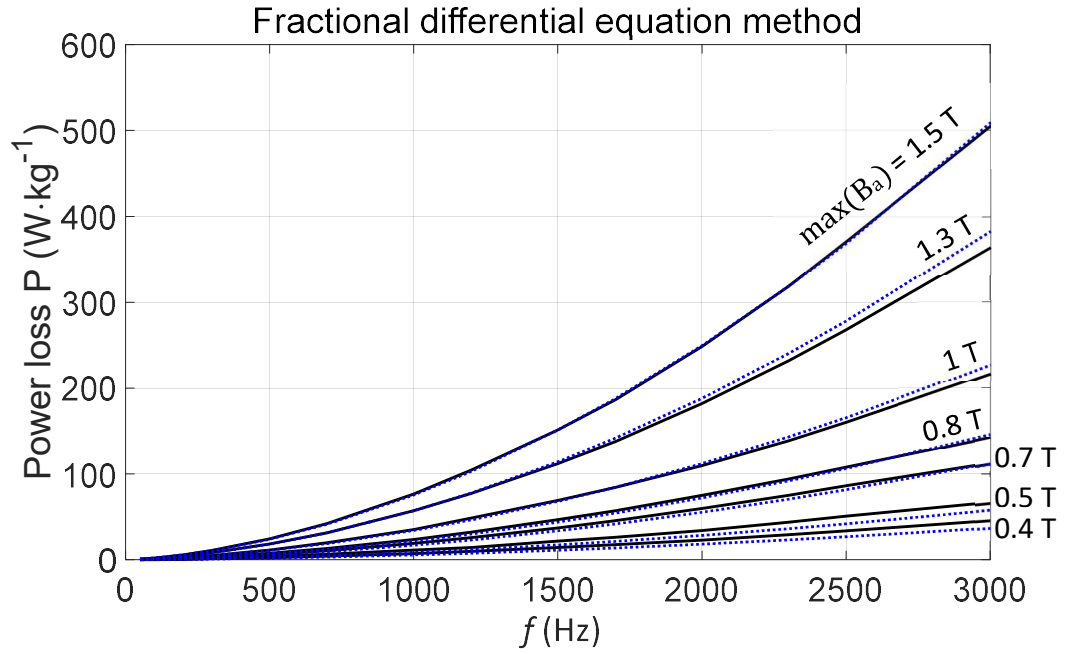

Fig. 9 – Comparison of simulations (fractional differential equation)/experimental results for the magnetic power loss in a GO FeSi specimen.

4.2 - Ferromagnetic Cole–Cole model

ImS is popular for characterizing ferroelectric materials. In this context, we used ImS (also termed dielectric spectroscopy) to observe the frequency dependence of the permittivity $\varepsilon(\omega)$, where $\omega = 2\pi f$ is the angular frequency.

Concomitantly to the development of ImS, researchers have developed simulation tools to improve their understanding and physical interpretations of ferroelectric materials. These simulation tools include the simple Debye equation [47], which works in ideal situations; but in most work, the fractional Cole–Cole model (Eq. (11)) is more effective [48][49]:

$$\boldsymbol{\varepsilon} = \varepsilon' - j\varepsilon'' = \varepsilon_\infty + \frac{\varepsilon S - \varepsilon\infty}{1+(j\omega\tau)^n}, \tag{11}$$

where ε_∞ is the high-frequency permittivity modulus, ε_S is the quasi-static permittivity, τ a characteristic relaxation time, and n is linked to the distribution of relaxation times ($0 < n < 1$). The observation of the Cole–Cole quantities ε', ε'', and Cole–Cole plots $\varepsilon''(\varepsilon')$ leads to an evident analogy with the ferromagnetic results ([50][51], and Figs. 3 and 4). The scientific literature has used this analogy, which leads to the magnetic Cole–Cole expression (Eq. (12)):

$$\boldsymbol{\mu} = \mu' + j\mu'' = \mu_\infty + \frac{\mu S - \mu\infty}{1+(j\omega\tau)^n}, \tag{12}$$

where μ_∞ is the high-frequency permeability modulus, and μ_S is the quasi-static permeability. In Ref. [50], Eq. (12) was used to measure the frequency dependence of magnetic fluids and in Ref. [51] for that of spin glasses.

4.3 - From a fractional differential equation to a ferromagnetic Cole–Cole model

Eq. (10) gives accurate results for simulations of the dynamical hysteresis cycles. Eq. (12) is valid for harmonic-type signals. We next establish a relationship between these equations.

During the impedance analyzer test, the magnetic flux density $\mathbf{B_a}$ generated in the tested specimen is supposed to have a harmonic-type waveform:

$$\mathbf{B}_a = B_0 \cos(\omega t). \tag{13}$$

We neglect the quasi-static loss contribution, so $\mathbf{B}_a$ and H_{stat} are considered as linearly linked:

$$H_{stat} = \frac{B_0 \cos(\omega t)}{\mu_{stat}}. \tag{14}$$

$\mathbf{B}_a$ is harmonic, and therefore the dynamic contribution in Eq. (10) (i.e., the product of ρ and the time-fractional derivation of $\mathbf{B}_a$) can be expressed analytically:

$$\rho \frac{d^n \mathbf{B}_a}{dt^n} = \rho B_0 \omega^n \cos\left(\omega t + n\frac{\pi}{2}\right). \tag{15}$$

A combination of Eqs. (10), (14), and (15) leads to an analytical expression for $\mathbf{H}_{surf}$:

$$\mathbf{H}_{surf} = \rho B_0 \omega^n \cos\left(\omega t + n\frac{\pi}{2}\right) + \frac{B_0 \cos(\omega t)}{\mu_{stat}}. \tag{16}$$

Eq. (16) can also be written using the complex number formalism:

$$\mathbf{H}_{surf} = B_0 e^{j\omega t} \cdot \left[\frac{1}{\mu_{stat}} + \rho \omega^n e^{jn\frac{\pi}{2}}\right], \tag{17}$$

where one can express $\boldsymbol{\mu}$, the complex permeability, as follows:

$$\boldsymbol{\mu} = \frac{\mathbf{H}_{surf}}{B_0 e^{j\omega t}} = \frac{1}{\frac{1}{\mu_{stat}} + \rho \omega^n e^{jn\frac{\pi}{2}}} = \frac{\mu_{stat}}{1 + (\tau \omega j)^n} \tag{18}$$

$$\tau^n = \mu_{stat} \cdot \rho. \tag{19}$$

Eqs. (18) and (12) are slightly different; but considering that μ_∞ (the infinite permeability associated with the high-frequency behavior and the spontaneous rotation magnetization mechanism) is ω-independent and close to zero (L' decreases highly in the high-frequency range in Fig. 4), we established the correspondence:

$$\boldsymbol{\mu} = \mu_\infty + \frac{\mu_{stat} - \mu_\infty}{1 + (j\omega\tau)^n} \approx \frac{\mu_{stat}}{1 + (\tau\omega)^n}. \tag{12}$$

From Eqs. (12)–Eq. (19), analytical development is an additional indicator that the magnetic Cole–Cole expression (Eq. (12)) is the low-amplitude harmonic version of the lumped fractional differential equation used to simulate the high-amplitude, frequency-dependent magnetic hysteresis cycles. From an experimental standpoint, however, the acquisition of the sinusoidal $\mathbf{B}_a$-imposed hysteresis cycles is complex because so doing requires highly sophisticated feedback control. In contrast, impedance measurements are easy, fast, and require standard equipment. Setting the dynamic simulation parameters (τ, ρ) by using IS and anticipating the dynamic loss and behavior in simulation is an alternative method that we validate for electrical steel in the last subsections of this manuscript.

4.4 – Theoretical expression of the dynamical losses under harmonic-type conditions

When the harmonic waveform condition is valid, Eqs. (11) and (13) are equivalent. Researchers have used both of these equations to derive an expression of the frequency-dependent loss contributions ($W_{dyn} = W_{cl} + W_{ex}$, in the STL domain of validity [4][41]).

In Eq. (10), the dynamic contribution relies exclusively upon the $\rho \cdot d^n\mathbf{B}_a/dt^n$ term, the dynamic loss can be obtained as follows:

$$W_{dyn} = \int_0^{1/f} \rho \frac{d^n\mathbf{B}_a}{dt^n} \cdot \frac{d\mathbf{B}_a}{dt} dt, \tag{20}$$

where if $\mathbf{B}_a$ is sinusoidal, there is an analytical solution for Eq. (20); and after simplifications leads to the following:

$$W_{dyn} = \pi\rho B_0^2 \omega^n \sin\left(n\frac{\pi}{2}\right). \tag{21}$$

In similar conditions, for the calculus of the dynamic losses using Eq. (12), it is necessary to express first, μ' and μ'':

$$\mu' = \frac{\mu_{stat} \cdot \left(1 + \omega^n \tau^n \cos\left(n\frac{\pi}{2}\right)\right)}{1 + 2\omega^n \tau^n \cos\left(n\frac{\pi}{2}\right) + \omega^{2n} \tau^{2n}} \tag{22}$$

$$\mu'' = -\frac{\mu_{stat} \cdot \left(\omega^n \tau^n \sin\left(n\frac{\pi}{2}\right)\right)}{1 + 2\omega^n \tau^n \cos\left(n\frac{\pi}{2}\right) + \omega^{2n} \tau^{2n}} \tag{23}$$

$\mathbf{B}_a$ and $\mathbf{H}_{surf}$ are harmonic:

$$\mathbf{B}_a = (\mu' + j\mu'') \cdot \mathbf{H}_{surf} \tag{24}$$

$$W_{dyn} = \int_0^T \mathbf{H}_{surf} \cdot \frac{d\mathbf{B}_a}{dt} dt \tag{25}$$

$$W_{dyn} = \frac{\pi B_0^2 \mu''}{\mu'^2 + \mu''^2}. \tag{26}$$

For $\mathbf{B}_a$ = 1.5 cos(ωt)-imposed conditions, ρ = 0.83 A·s^n·T^{-n}·m^{-1}, μ_{stat} = 10000 μ_0, and n ∈ [0 to 1] as the resolution of Eqs. (21) and (26) give superimposed results; indicated in Fig. 10 and confirming that both models can be used to predict the frequency-dependent core losses.

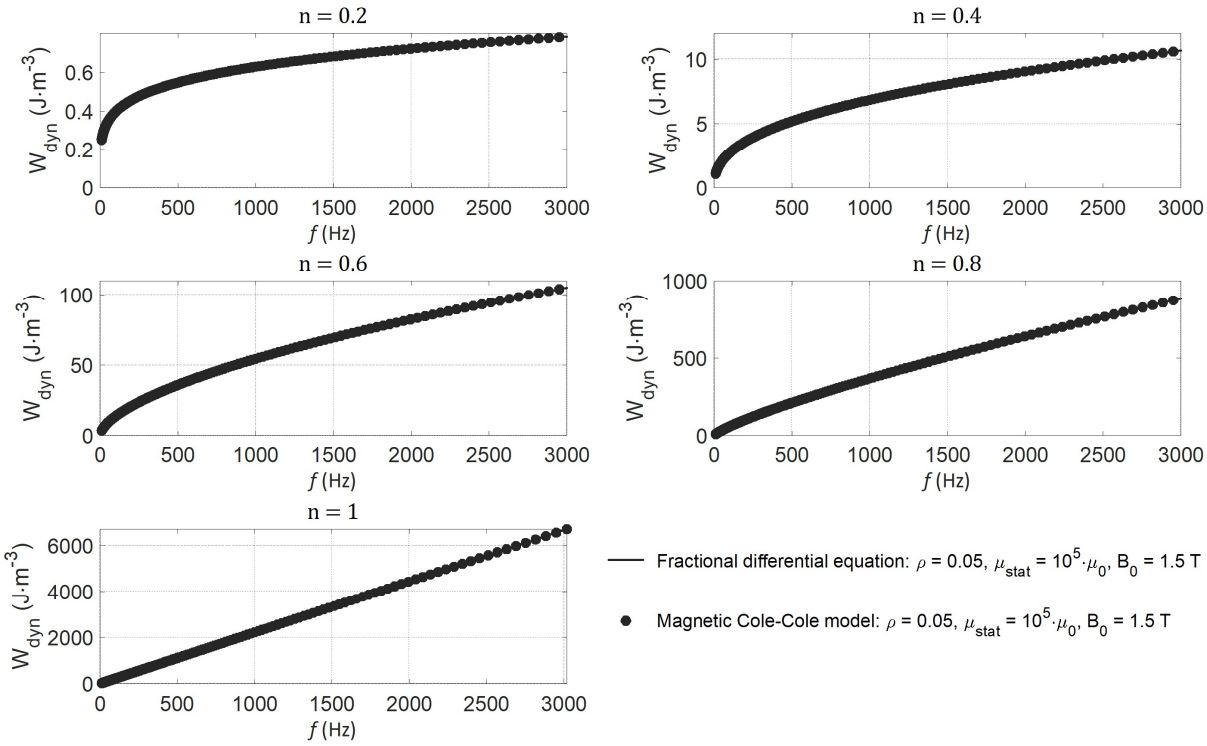

Fig. 10 – Magnetic loss as obtained from the fractional differential equation and the magnetic Cole–Cole model.

4.5 – Comparison with experimental results and validation of inductance spectroscopy

The resolution of Eq. (10) for electrical steel GO FeSi specimens gives precise simulation results: $\rho = 0.05\ A \cdot s^{n} \cdot T^{-n} \cdot m^{-1}$ and $n = 0.83$ (Figs. 8 and 9). The same parameters can be used in the Cole–Cole model (Eq. (12)) and for a given μ_{stat} lead to the simulation of μ' and μ'' vs. *f*.

To compare with the experimental results shown in Figs. 4 or 5, a relationship between the magnetic permeability and the inductance is necessary. In Ref. [20], researchers used Eq. (27):

$$(\mu' + j\mu'') = G \cdot (L' + jL''), \tag{27}$$

where G is a constant ($G = 10^{8}\ m^{-1}$, for wires and microwires [20]).

Ref. [40] describes (for various geometries) the theoretical relationships between $\boldsymbol{\mu}$ and $\mathbf{L}$ in the absence and presence of macroscopic eddy currents. By assuming that the width of our tested strips is sufficiently large compared with the thickness, they can be assimilated to the slab studied in Ref. [40]. The Cole–Cole formalism (Eq. (12)) takes into account the eddy currents' contribution, and $\boldsymbol{\mu}$ and $\mathbf{L}$ can be linked using the relationship that corresponds to the absence of eddy currents:

$$(\mu' + j\mu'') = \frac{6b}{a \cdot c} \cdot (L' + jL''), \tag{28}$$

where $a = d/2$, b, and c are the tested strips' half-thickness, width, and length, respectively. We compared the simulation results with the experimental results in Fig. 11. To be consistent with the experimental conditions, the experimental results are those of Fig. 4; that is, the electrical current is in the TD and the magnetic excitation in the RD. $\sigma = 2.2 \times 10^{6}\ S \cdot m^{-1}$. We tested max(I) = 2 and 100 mA sinusoidal imposed excitations to check the viability under extreme conditions.

We set the static permeability $\mu_{stat} = 8330 \cdot \mu_0$ for the max(I) = 2 mA simulations, $\mu_{stat} = 21750\ \mu_0$ for the max(I) = 100 mA simulations, and μ_∞ to $\mu_\infty = 1450\ \mu_0$ based on the experimental

observations in the low- and high-frequency range. Even if minor differences, probably because of small divergence between the GO FeSi specimens tested, can be observed, the overall results (analytical solution Eq. 12 in the [10^2-10^6] frequency range) confirm the conservation of the dynamical behavior between the testing situations and the reliability of IS as a dynamical behavior characterization method.

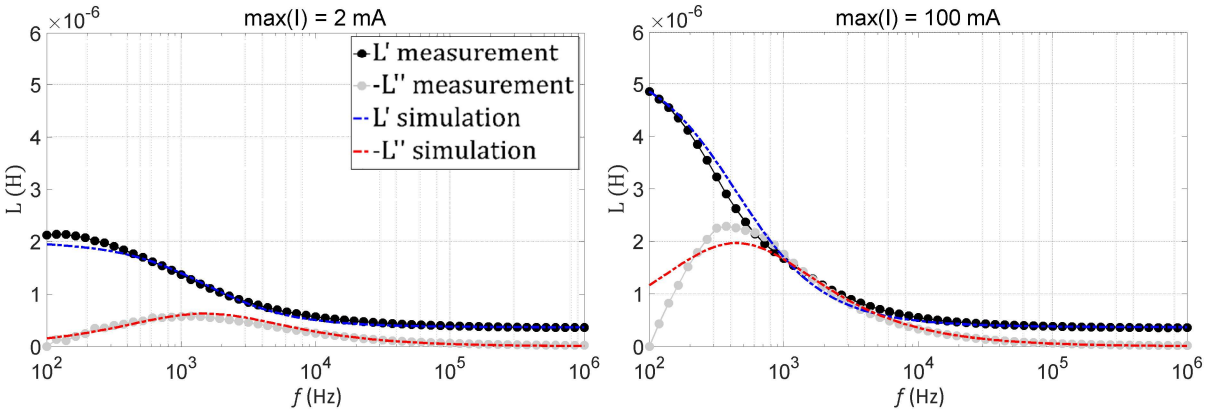

Fig. 11 – Comparison of simulations (Cole–Cole model: ρ = 0.05 A·s^n·T^{-n}·m^{-1} and n = 0.83) / measurements (IS).

An optimization process based on minimization of the mean relative standard deviation error function (Eq. (29)) can also be run to reach the best combination of parameters:

$$\text{Err}\,(\%) = \frac{100}{4q}\sum_{i=1}^{q}\frac{\left|L'_{imeas}(f_i)-L'_{isim}(f_i)\right|}{L'_{imeas}(f_i)}_{max(I)=2mA} + \frac{\left|L''_{imeas}(f_i)-L''_{isim}(f_i)\right|}{L''_{imeas}(f_i)}_{max(I)=2mA} + \frac{\left|L'_{imeas}(f_i)-L'_{isim}(f_i)\right|}{L'_{imeas}(f_i)}_{max(I)=100mA} + \frac{\left|L''_{imeas}(f_i)-L''_{isim}(f_i)\right|}{L''_{imeas}(f_i)}_{max(I)=100mA} \quad (29)$$

We obtained the combination that gives the minimum error (≈ 9 %) when ρ = 0.07 A·s^n·T^{-n}·m^{-1}, n = 0.79, μ_{stat} = 8510 · μ_0 (max(I) = 2 mA), and μ_{stat} = 24100 · μ_0 (max(I) = 100 mA). Fig. (12) shows a comparison of simulations vs. measurements in this optimal configuration.

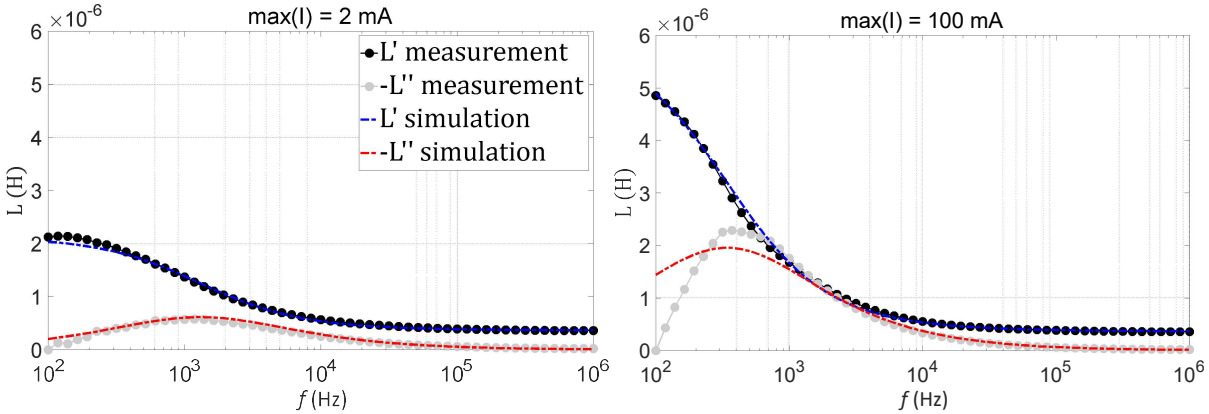

Fig. 12 – Comparison of simulations (Cole–Cole model: $\rho = 0.07\ A{\cdot}s^{n}{\cdot}T^{-n}{\cdot}m^{-1}$ and $n = 0.79$) / measurements for IS observations.

5 – Discussion and conclusion

IS is a valuable experimental method to collect dynamic information of magnetization mechanisms. Among those mechanisms, some of them have well-assessed frequency dependency, whereas others are not clear, such as :

- The macroscopic eddy current contribution frequency dependency is well known and can be expressed analytically (Eq. (4)).
- Domain wall bulging is inevitable even under low-amplitude excitation. The plateau-like behavior visible in the low-frequency range of L' in Fig. 5 is characteristic of this mechanism. The right limit of this plateau, when the frequency rises, gives information about this mechanism time constant. It confirms that beyond a frequency threshold, the excitation frequency is too high to trigger this mechanism, ending with a decrease of L'.
- Ref. [20] indicates that the rotation magnetization phenomenon exhibits the shortest time constant. This mechanism is not associated with the magnetic domain kinetic but with the atomic magnetic moments. Rotation magnetization is characterized by the

plateau-like behavior that is evident in Figs. 4 and 5 for L' in both the TD and RD directions and frequencies higher than a few kilohertz. The magnetization rotation time constant is low enough that even the highest frequency tested in this study can trigger this mechanism. In this very-high frequency range, it is the only remaining magnetization mechanism and maintains a nonzero L' value. A decrease of L' is forecasted at an even higher frequency level but not tested in the framework of this study.

- The irreversible domain wall motions, avalanche, and ripple phenomena can be grouped into the same category: domain wall kinetics. These mechanisms are strongly frequency-dependent. Together with the macroscopic eddy currents, they contribute to the substantial decrease of the real part of the permeability: μ' (Fig. 4; from a few hundred kilohertz to a few kilohertz).

In this study, we verified that researchers can adapt simulation tools used in ferroelectricity research (the Cole–Cole model) to simulations of IS for electrical steel specimens. We presented the relationships between this model and the fractional differential equation used for the frequency dependence of the dynamic hysteresis. A combination of parameters that give correct simulation results in both experimental situations gives almost the same combination of parameters. This observation confirms that IS can be used to set dynamic parameters; which is useful for predicting the frequency dependence of hysteresis cycles observed under various experimental conditions, such as those defined in characterization standards (e.g., Epstein frame and single-sheet tester).

IS also facilitates access in a straightforward manner to the high-frequency range where the classic methods have limitations.

There are various possibilities for future work. It would be interesting to check the viability of the proposed method on various experimental conditions (e.g., local electrical contacts such as point probes, solving the geometrical restriction issue associated with the strips, and easing the industrial implementation). Furthermore, the capability of IS to isolate the magnetization mechanisms and the influence of the directionality is worthy of additional investigation. In this study, we tested the frequency dependency of these mechanisms, but these mechanisms can also be studied as the function of other parameters; including the temperature, mechanical stress, plastic strain, or even micro-structural content. By checking the sensitivity for each magnetization mechanism, specific indicators that correspond to higher sensitivity could be selected and IS used as an indirect means of assessing these quantities.

Acknowledgments

This work is supported by the LyC collaborative research project 2021 of the Institute of Fluid Science, Tohoku University (J21Ly11).

References:

[1] H. Herring, “Energy efficiency – a critical view,” *Energy*, vol. 31, iss. 1, pp. 10 – 20, 2006.

[2] G.N. Smirnova, B. Yu, V.Y. Neyman, “New principles and ways of increase of energy efficiency of electromagnetic machines,” 2006 international forum on strategic technology, pp. 314 – 315, 2006.

[3] R.M. Bozorth, “Magnetism,” Enc. Brit., vol. 14, pp. 636 - 667, 1957.

[4] G. Bertotti, “Hysteresis in Magnetism,” San Diego, CA, USA: Academic, 1998.

[5] S.M. Plotnikov, “Determination of eddy-current and hysteresis losses in the magnetic circuits of electrical machines,” *Meas. Tech.*, vol. 63, pp. 904 – 909, 2021.

[6] F. Irannezhad, H. Heydari, F. Faghihi, “Precise appraisement of the harmonic loads impact on hysteresis losses in a 3-phase HTS transformer,” *Int. J. of elect. Pow. & Energ. Syst.*, vol. 133, 2021.

[7] A. Magni., A. Sola, O. de la Barrière, E. Ferrara, L. Martino, C. Ragusa, C. Appino, F. Fiorillo, “Domain structure and energy losses up to 10 kHz in grain-oriented Fe-Si sheets,” *AIP Advances*, vol. 11, 015220, 2021.

[8] B. Ducharne, P. Tsafack, Y.A. Tene Deffo, B. Zhang, G. Sebald, “Fractional operators for the magnetic dynamic behavior of ferromagnetic specimens: An overview,” *AIP Advances*, vol. 11, 035309, 2021.

[9] L. Moreira Duarte, J. Daniel de Alencar Santos, F. Nélio Costa Freitas, P. Pedrosa Rebouças Filho, H. Ferreira Gomes de Abreu, “A novel approach based on pattern recognition techniques to evaluate magnetic properties of a non-grain oriented electrical steel in the secondary recrystallization process,” *Measurement*, vol. 167, 108135, 2021.

[10] H. Zhao, H.H. Eldeeb, Y. Zhang, D. Zhang, Y. Zhan, G. Xu, O. A. Modhammed, “ An improved core loss model of ferromagnetic materials considering high-frequency and nonsinusoidal supply,” *IEEE Trans. Ind. App.*, vol. 57, n° 4, pp. 4336 – 4346, 2021.

[11] N.P. Goss, US Patent, N° 1,965,559, 1934.

[12] R. Findlay, R. Belmans, D. Mayo, “Influence of the stacking method on the iron losses in power transformer cores,” *IEEE Trans. Magn.,* vol. 26, n° 5, pp. 1990 – 1992, 1990.

[13] B. Weidenfeller, W. Riehemann, “Effects of surface treatments on the hysteresis losses of GO iron silicon steel,” *J. Magn. Magn. Mater.,* vol. 292, pp. 210 – 214, 2005.

[14] The world databank: https://data.worldbank.org

[15] M. Chen, H.V. Poor, “High-frequency power electronics at the grid edge: A bottom-up approach toward the smart grid,” *IEEE Electrification magazine*, vol. 8, n° 3, 2020.

[16] X. Yu, C. Cecati, T. Dillon, M.G. Simões, "The new frontier of smart grids," *IEEE Industrial Electronics Magazine*, vol. 5, n° 3, pp. 49 – 63, 2011.

[17] IEC 60404-2, "Magnetic materials – Part 2: Methods of measurement of the magnetic properties of electrical steel strip and sheet by means of an Epstein frame," *International Electrotechnical Commission*, June 2008.

[18] IEC 60404-3, "Magnetic materials – Part 3: Methods of measurement of the magnetic properties of electrical steel strip and sheet by means of a single sheet tester," *International Electrotechnical Commission*, April 2010.

[19] IEC 60404-6, "Magnetic materials – Part 6: Methods of measurement of the magnetic properties of magnetically soft metallic and powder materials at frequencies in the range 20 Hz to 200 kHz by the use of ring specimens," *International Electrotechnical Commission*, June 2003.

[20] I. Betancourt, "Magnetization dynamics of amorphous ribbons and wires studied by inductance spectroscopy," *Materials*, vol. 4, pp. 37 – 54, 2011.

[21] A.S. Hamdy, E.E. Shenawy, T.E. Bitar, "Electrochemical impedance spectroscopy study of the corrosion behaviour of some niobium bearing stainless steels in 3.5% NaCl," Int. J. of Electrochemical Sci., vol. 1, pp. 171 – 180, 2006.

[22] J.T.S. Irvine, D.C. Sinclair, A.R. West, "Electroceramics: characterization by impedance spectroscopy," Adv. Mater., vol. 2, pp. 132 – 138, 1990.

[23] M.M. Musiani, "Characterization of electroactive polymer layers by electrochemical impedance spectroscopy (EIS)," Electrochimica Acta, vol. 35, iss. 10, pp. 1665 – 1670, 1990.

[24] E. Barsoukov, J.R. Macdonald, "Fundamentals of impedance spectroscopy," in: J.W. & Sons (Ed.), Impedance spectroscopy theory, experiment, and application, second ed., pp. 1 – 26, 2018.

[25] G. T. Rado, "Magnetic spectra of ferrites," *Rev. Mod. Phys.*, vol. 25, iss. 81, 1953

[26] J.T.S. Irvine, A.R. West, E. Amano, A. Huanosta, R. Valenzuela, "Characterization of magnetic materials by impedance spectroscopy," *Solid State Ionics,* vol. 40 – 41, part. 1, pp. 220 – 223, 1990.

[27] R. Amano, R. Velenzuela, J.T.S. Irvine, A.R. West, "Domain wall relaxation in amorphous ribbons," *J. Appl. Phys.*, vol. 67, pp. 5589 – 5591, 1990.

[28] H. Montiel, G. Alvarez, M.P. Gutiérrez, R. Zamorano, R. Valenzuela, "The effect of metal-to-glass ratio on the low field microwave absorption at 9.4 GHz of glass-coated CoFeBSi microwires," *IEEE Trans. Magn.,* vol. 42, n° 10, pp. 3380 – 3382, 2006.

[29] R. Valenzuela, I. Betancourt, "Giant magnetoimpedance, skin depth, and domain wall dynamics," *IEEE Trans. Mag.*, vol. 38, iss. 5, pp. 3081 – 3083, 2002.

[30] F. Qiu, M.J. Klug, G. Tian, P. Hu, J. McCord, “Influence of magnetic domain wall orientation on Barkhausen noise and magneto-mechanical behavior in electrical steel,” *J. Phys. D: App. Phys.*, vol. 52, 265001, 2019.

[31] M. Carara, M. N. Baibich, R. L. Sommer, “Magnetization dynamics as derived from magneto impedance measurements,” *J. App. Phys.*, vol. 88, n°1, pp. 331 – 335, 2000.

[32] S.E. Zirka, Y.I. Moroz, P. Marketos, A.J. Moses, “Viscosity-based magnetodynamic model of soft magnetic materials,” *IEEE Trans. Mag.*, vol. 42, n°9, pp. 2121 – 2132, 2006.

[33] M.A. Raulet, B. Ducharne, J.P. Masson, and G. Bayada, “The magnetic field diffusion equation including dynamic hysteresis: a linear formulation of the problem,” *IEEE Trans. Mag.,* Vol. 40, n° 2, pp. 872-875, 2004.

[34] M. Petrun, S. Steentjes, “Iron-loss and magnetization dynamics in non-oriented electrical steel: 1-D Excitations up to high frequencies,” *IEEE Access*, vol. 8, pp. 4568 – 4593, 2020.

[35] C. Appino, O. de la Barrière, F. Fiorillo, M. LoBue, F. Mazaleyrat, C. Ragusa, “Classical eddy current losses in soft magnetic composites,” *J. App. Phys.*, vol. 113, 17A322, 2013.

[36] M.L. Sancher, R. Valenzuela, M. Vasquez, A. Hernando, “Circumferential permeability in non-magnetostrictive amorphous wires,” *J. Mater. Res.,* vol. 11, pp. 2486 – 2489, 1996.

[37] O. Hubert, L. Daniel, “Multiscale modeling of the magneto-mechanical behavior of grain-oriented silicon steels,” *J. Magn. Magn. Mater.,* vol. 320, pp. 1412 – 1422, 2008.

[38] A. Yashan, Measurements and semi-analytical modeling of incremental permeability using eddy current coil in the presence of magnetic hysteresis, in: F. Kojima, T. Takagi, S.S. Udpa, J. Pávó (Eds.), Electromagnetic Nondestructive Evaluation (VI), IOS press, pp. 150 – 157, 2002.

[39] T. Matsumoto, T. Uchimoto, T. Takagi, G. Dobmann, B. Ducharne, S. Oozono, H. Yuya, “Investigation of Electromagnetic Nondestructive Evaluation of Residual Strain in Low Carbon Steels Using the Eddy Current Magnetic Signature (EC-MS) Method,” *J. Magn. Magn. Mater.,* Vol. 479, pp. 212 – 221, 2019.

[40] D.-X. Chen, J.L. Muñoz, “AC impedance and circular permeability of slab and cylinder,” *IEEE Trans. Magn.,* vol. 35, n° 3, pp. 1906 – 1923, 1999.

[41] G. Bertotti, “General properties of power losses in soft ferromagnetic materials,” *IEEE Trans. Magn.,* vol. 24, n° 1, pp. 621 – 630, 1988.

[42] S.E. Zirka, Y.I. Moroz, P. Marketos, A.J. Moses, “Viscosity-based magnetodynamic model of soft magnetic materials,” *IEEE Trans. Magn.,* vol. 42, n° 9, pp. 2121 – 2132, 2006.

[43] B. Zhang, B. Gupta, B. Ducharne, G. Sebald, T. Uchimoto, “Preisach’s model extended with dynamic fractional derivation contribution,” *IEEE Trans. Magn.,* Vol. 54, n° 3, pp. 1 – 4, 2018.

[44] B. Zhang, B. Gupta, B. Ducharne, G. Sebald, T. Uchimoto, “Dynamic magnetic scalar hysteresis lump model, based on Jiles-Atherton quasi-static hysteresis model extended with dynamic fractional derivative contribution,” *IEEE Trans. Magn.,* vol. 54, n° 11, pp. 1 – 4, 2018.

[45] R. Liu, L. Li, “Analytical prediction of energy losses in soft magnetic materials over broadband frequency range,” *IEEE Trans. Power Electron.,* vol. 36, n° 2, pp. 2009 – 2017, 2021.

[46] B. Ducharne, G. Sebald, “Fractional prediction of energy losses in soft magnetic materials over broadband frequency range: a leap forward,” *Commun. Nonlinear Sci. Numer. Simulat.*, under revesion, 2021.

[47] P. Debye, “Zur theorie der anomalen dispersion im gebiete der langwelligen elektrishen,” *Strahlung. Ver. Deut. Phys. Gesell.*, vol. 15, pp. 777 – 793, 1913.

[48] K.S. Cole, R.H. Cole, “Dispersion and absorption in dielectrics – I alternating current characteristics,” *J. Chem. Phys.*, vol. 9, pp. 341 – 352, 1941.

[49] K.S. Cole, R.H. Cole, “Dispersion and absorption in dielectrics – II Direct current characteristics,” *J. Chem. Phys.*, vol. 10, pp. 98 – 105, 1942.

[50] R. Valenzuela, H. Montiel, M.P. Gutiérrez, I. Betancourt, “Characterization of soft ferromagnetic materials by inductance spectroscopy and magnetoimpedance,” *J. Magn. Magn. Mater.,* Vol. 294, pp. 239 – 244, 2005.

[51] R. Valenzuela, “Low-frequency magnetoimpedance: domain wall magnetization process,” *Phys. B*, vol. 299, pp. 280 – 285, 2001.